

Circular orbits and accretion disk around a deformed-Schwarzschild black hole in loop quantum gravity

Kourosh Nozari,^{1,*} Sara Saghafi,^{1,†} Milad Hajebrahimi,^{1,‡} and Kimet Jusufi^{2,§}

¹*Department of Theoretical Physics, Faculty of Science,*

University of Mazandaran, P. O. Box 47416-95447, Babolsar, Iran

²*Physics Department, University of Tetova, Ilinden Street nn, 1200, Tetovo, North Macedonia*

In this paper, we study the motion of neutral and electrically charged particles in the vicinity of a deformed-Schwarzschild black hole inspired by Loop Quantum Gravity (LQG). To examine the motion of an electrically charged test particle, we propose an expression for electromagnetic 4-potential that contains the impacts of loop quantum gravity. This electromagnetic 4-potential satisfies approximately the covariant Maxwell's equations to first order in the loop quantum effects. We explore the effects of the loop quantum correction parameter on the particle geodesics. We investigate the innermost stable circular orbits (ISCOs) for both neutral and electrically charged particles in detail, demonstrating that the loop quantum parameter significantly influences on the ISCO radius, causing it to shrink. Finally, we explore the accretion disk around the loop quantum black hole. We delve into the electromagnetic radiation flux, temperature, differential luminosity, and the spectral luminosity as radiation properties of the accretion disk in detail. We show that the loop quantum correction parameter shifts the profile of the electromagnetic flux and accretion disk temperature towards the central object, leading to a slight increase in these quantities.

Keywords: Accretion Process, Accretion Discs, Loop Quantum Gravity, Black Hole Physics.

I. INTRODUCTION

Black holes are believed to originate from the gravitational collapse of massive, dense objects when their internal pressure can no longer counteract gravity. These enigmatic cosmic entities exhibit fascinating properties that continue to captivate researchers. Breakthroughs such as the detection of spacetime ripples [1, 2], high-resolution imaging by the Event Horizon Telescope [3, 4], and studies of accretion disk emissions [5–7] have opened new avenues for exploration. Such discoveries enable scientists to probe the unique characteristics and gravitational behavior of black holes within both classical and alternative frameworks of gravity. In particular, astrophysical black holes—those observed in nature—serve as natural laboratories for testing fundamental theories. Through multi-messenger astronomy, they provide crucial insights into quantum gravity and other modi-

fied gravitational models, offering a unique opportunity to validate theoretical predictions against observational data.

Although observational evidence strongly supports the existence of massive compact objects consistent with black holes, fundamental questions persist—particularly regarding the nature of their singularities. In gravitation theory and relativistic astrophysics, spacetime singularities, characterized by diverging curvature and density, remain a central topic of investigation. The singularity theorems established by Hawking and Penrose demonstrate that such singularities are an inevitable consequence of gravitational collapse under classical general relativity (GR). However, their presence challenges the predictive power of GR, particularly in extreme regimes. A further complication arises from the possibility of naked singularities—gravitational singularities not concealed by an event horizon. If such singularities were observable, they would violate cosmic censorship conjectures and potentially disrupt the deterministic framework of classical GR.

A robust theory of gravity must ultimately resolve the problem of spacetime singularities. Unifying quantum

* knozari@umz.ac.ir

† s.saghafi@umz.ac.ir

‡ m.hajebrahimi@stu.umz.ac.ir

§ kimet.jusufi@unite.edu.mk

mechanics with general relativity remains a key challenge in developing a quantum gravity framework. Among various quantum gravity approaches, loop quantum gravity (LQG) has emerged as a leading candidate, with significant theoretical advancements [8–14]. Studies on spherically symmetric black holes within LQG have revealed novel quantum corrections [15–25]. These corrections suggest that the classical singularity in Schwarzschild black holes may be resolved, though the exact mechanism depends on the quantization scheme. Notably, LQG predicts that quantum geometry effects can replace cosmological singularities, such as the Big Bang, with a nonsingular bounce [26, 27], leading to improved black hole models [28–30]. Recent work on the quantum Oppenheimer–Snyder (qOS) model in loop quantum cosmology has introduced a new black hole solution that eliminates the Schwarzschild singularity via an intermediate transition region with an inner horizon [22]. While the exterior geometry resembles a deformed Schwarzschild spacetime, this quantum-corrected black hole exhibits distinct observational signatures, particularly in shadow formation and stability [31, 32], where discrepancies were observed in asymptotically flat spacetimes. Further extensions include a qOS model with a positive cosmological constant [33] as well as investigations into anti-de Sitter [34] and higher-dimensional [35] spacetimes, broadening the scope of LQG-inspired black hole thermodynamics and dynamics..

This work explores a loop quantum gravity (LQG)-inspired deformed Schwarzschild black hole, analyzing how its quantum correction parameter influences spacetime geometry. To understand these modifications, we investigate the dynamics of both neutral and charged particles orbiting this quantum-corrected black hole. Additionally, we examine the properties of accretion disks around such black holes, providing insights into their observable characteristics and distinguishing features compared to classical Schwarzschild black holes. By studying particle motion and accretion processes, we aim to uncover observable signatures of LQG effects, potentially offering new ways to test quantum gravity predictions in astrophysical settings..

The investigation of gravity and spacetime geometry in the strong-field regime is expected to benefit significantly from both theoretical and observational studies

of accretion disks around black holes. These disks not only offer a window into the intense gravitational fields near black holes but also serve as natural laboratories for probing high-energy astrophysical phenomena that remain poorly understood [36]. Because the strong gravity near a black hole can drastically influence the paths of test particles, it can alter observable properties such as disk parameters and the location of the innermost stable circular orbit (ISCO). Therefore, the reliability of data obtained from observations of accretion disks becomes critically important. Specifically, the thermal emission from thin accretion disks offers a powerful tool for testing gravitational theories in strong-field conditions. Motivated by this perspective, we analyze a compelling solution derived from loop quantum gravity (LQG), based on a quantum version of the Oppenheimer–Snyder collapse scenario within loop quantum cosmology. By applying the Novikov–Thorne formalism for geometrically thin, optically thick disks, we explore the radiative properties and distinctive signatures of the accretion disk surrounding this loop quantum black hole. Furthermore, we investigate the ISCOs associated with this model, shedding light on how quantum gravitational corrections may affect observable disk structures.

The remainder of this paper is organized as follows. In the next section, we present a brief review of the qOS model [22] and the corresponding modified metric inspired by LQG. The motion of neutral test particles is examined in Sec. III, and in Sec. IV, the dynamics of electrically charged particles surrounding the loop quantum black hole are examined. Section V focuses on the geometrically thin Novikov–Thorne model for the accretion disk surrounding the loop quantum black hole which is followed by covering the temperature profile, differential luminosity, radiative efficiency, and radiant energy flux over the accretion disk. Our findings have been gathered in Sec. VI. We utilize the $(-, +, +, +)$ signature for the spacetime metric throughout this study.

II. DEFORMED-SCHWARZSCHILD BLACK HOLE IN LQG

The four-dimensional quantum Oppenheimer–Snyder model [22, 32] begins with an effective inner spacetime area that contains corrections of loop quantum cosmology

(LQC) [10]. The effective interior spacetime area is then matched with an outside spacetime region via junction conditions on their common boundary surface.

In particular, in Ref. [10] authors show that the Ashtekar–Pawlowski–Singh (APS) dust particles move along geodesics while maintaining constant \tilde{r} , θ , and φ (the coordinate \tilde{r} is used in the ball region only [10]), forming a dust sphere within the range $0 \leq \tilde{r} \leq \tilde{r}_0$. Then, authors in Ref. [22] for the qOS model assumes a (pseudo)-static, spherically symmetric metric

$$ds^2 = -(1 - F(r))dt^2 + (1 - G(r))^{-1}dr^2 + r^2d\Omega^2, \quad (1)$$

where $d\Omega^2 = d\theta^2 + \sin^2\theta d\varphi^2$ is the line element of unite 2-sphere while $F(r)$ and $G(r)$ are two unknown functions of r . The coordinates (t, r) describe the exterior region, while (\tilde{t}, \tilde{r}) are used within the dust region. The junction conditions determine the metric, rather than the field equations. The resulting deformed Schwarzschild solution exhibits a black hole mass gap and an effective energy-momentum tensor, potentially establishing a connection between quantum black hole phenomena and dark matter.

Loop Quantum Cosmology (LQC) approaches have been applied to black hole models; however with diverse interpretations. Some propose a bouncing interior that eliminates the Killing horizon, leading to black hole evaporation. Others suggest that the black hole transits into a white hole through quantum tunnelling. Certain models preserve the exterior structure while replacing singularities with regular edges, enabling multiple Kruskal-like extensions.

A complementary scenario, known as the quantum Swiss Cheese (qSC) model, considers an empty bubble ($0 \leq \tilde{r} \leq \tilde{r}_0$) embedded within the APS quantum universe. As the universe contracts, the bubble shrinks, potentially forming a black hole unless its size approaches the Planck scale.

Both models rely on the dust surface at $\tilde{r} = \tilde{r}_0$, which is matched across the APS and exterior metrics through the identification $(\tilde{t}, \tilde{r}_0, \theta, \varphi) \sim (t(\tilde{t}), r(\tilde{t}), \theta, \varphi)$. Ensuring the continuity of the induced metric and extrinsic curvature determines the functions $F(r)$ and $G(r)$, as well as the trajectory of the dust surface, allowing for the derivation of (1) as the line element of the deformed-Schwarzschild black hole in LQG (dubbed as loop quan-

tum black hole)

$$ds^2 = -f(r)dt^2 + f^{-1}(r)dr^2 + r^2d\Omega^2, \quad (2)$$

$$f(r) = 1 - \frac{2GM}{r} + \frac{\alpha G^2 M^2}{r^4},$$

where $\alpha = 16\sqrt{3}\pi\gamma^3\ell_P^2$ in which ℓ_P represents the Planck length and γ is the Barbero–Immirzi parameter. In Ref. [22] the authors identified a straightforward method to determine the functions $F(r)$ and $G(r)$ (see Appendix A of Ref. [22] for more details). One can see that the metric tensor $g_{\alpha\beta}$ associated with the line element of the loop quantum black hole (2) has the following non-zero components

$$g_{tt} = -f(r), \quad g_{rr} = f^{-1}(r), \quad (3)$$

$$g_{\theta\theta} = r^2, \quad g_{\varphi\varphi} = r^2 \sin^2\theta.$$

It is important to note that the form of the metric in equation (2) is determined for

$$r > r_b = \left(\frac{\alpha GM}{2}\right)^{1/3}. \quad (4)$$

The dust surface radius $a(\tau)r_0$ of Ref. [10] spans the interval $[r_b, \infty]$. Consequently, as in Ref. [22], the functions $F(r)$ and $G(r)$ can be specified arbitrarily for $r < r_b$. The parameter M corresponds to the ADM mass of the metric tensor (2).

In Ref. [22], the authors demonstrated that the global structure of spacetime, as described by Eq. (2), depends on the number of roots of $(1 - F(r))$. They introduced the parameter $0 < \beta < 1$ as

$$G^2 M^2 = \frac{4\beta^4}{(1 - \beta^2)^3} \alpha. \quad (5)$$

For $0 < \beta < 1/2$, we have

$$M < M_{\min} := \frac{4}{3\sqrt{3}G}\sqrt{\alpha}, \quad (6)$$

According to [22], the function $(1 - F(r))$ does not have a real root, indicating that the metric (2) does not admit any horizon. The global causal structure of the maximally extended spacetime is therefore identical to that of Minkowski spacetime. Thus, the value

$$M_{\min} = \frac{16\gamma\sqrt{\pi\gamma}\ell_P}{3\sqrt{3}G}, \quad (7)$$

serves as a lower bound for black holes predicted by the models discussed in Ref. [22] (see [21, 37, 38] for compatible results). The minimum mass is approximately

equal to the Planck mass. Its precise value depends on the Barbero–Immirzi parameter γ of LQG, which is estimated to be around 0.2 [39, 40].

Consider $M > M_{\min}$, where $1/2 < \beta < 1$. The function $(1 - F(r))$ has precisely two roots

$$r_{\pm} = \frac{\beta (1 \pm \sqrt{2\beta - 1})}{\sqrt{(1 + \beta)(1 - \beta)^3}} \sqrt{\alpha}, \quad (8)$$

This makes t a singular coordinate. Thus, β acts as a dimensionless parameter that determines whether quantum effects permit or prevent the formation of an event horizon. It encapsulates the interplay between the black hole mass M and the quantum correction parameter α . In Ref. [22] the authors follow the same techniques as for the Reissner–Nordström (RN) metric to expand the metric tensor (2). They showed that the resulting Penrose diagram has a structure comparable to the RN spacetime.

This black hole’s (loop quantum black hole) properties were explored and shown to be stable under scalar and vector perturbations using quasinormal modes. The shadows were studied in Ref. [32]. The spacetime model has been applied to the LQG-AdS example, and its thermodynamics have been explored [34]. Also, in Ref. [35] the quantum Oppenheimer–Snyder model for higher-dimensional spacetimes was studied.

We further investigate the particle dynamics for two different cases around the deformed-Schwarzschild black hole in Loop Quantum Gravity. This is what we intend to examine in the next section.

III. THE MOTION OF NEUTRAL PARTICLES

In this study, the motion of a test particle is governed by the geodesic structure of the spacetime around a loop quantum black hole. Using the Lagrangian formalism, we investigate the time-like geodesics in the vicinity of the static, spherically symmetric loop quantum black hole. [41, 42].

Due to the spherical symmetry of this spacetime, the line element (2) of the loop quantum black hole, which includes the metric function $f(r)$ as shown in Eq. (2), remains invariant under both time translations and rotations about the symmetry axes. As a result, the spacetime of the loop quantum black hole possesses two Killing

vectors associated with these symmetries.

$$\begin{aligned} {}^{(t)}\zeta^\mu \frac{\partial}{\partial x^\mu} &= (1, 0, 0, 0) \frac{\partial}{\partial x^\mu} = \frac{\partial}{\partial t}, \\ {}^{(\varphi)}\zeta^\mu \frac{\partial}{\partial x^\mu} &= (0, 0, 0, 1) \frac{\partial}{\partial x^\mu} = \frac{\partial}{\partial \varphi}. \end{aligned} \quad (9)$$

Due to the spherical symmetry of this spacetime, the line element (2) of the loop quantum black hole, which includes the metric function $f(r)$ as shown in Eq. (2), remains invariant under both time translations and rotations about the symmetry axes. As a result, the spacetime of the loop quantum black hole possesses two Killing vectors associated with these symmetries.

The expression for the Lagrangian of a test particle moving through the loop quantum black hole’s spacetime is

$$\mathcal{L} = \frac{1}{2} g_{\mu\nu} \dot{x}^\mu \dot{x}^\nu, \quad (10)$$

where a derivative with respect to the affine parameter τ is represented by an over-dot. The test particle’s four-velocity is defined by the formula $\dot{x}^\mu \equiv u^\mu = (u^t, u^r, u^\theta, u^\varphi)$. With $\theta = \frac{\pi}{2}$, we are interested in the particle’s planar motion on the equatorial plane. Consequently, applying the Euler–Lagrange formula

$$\frac{d}{d\tau} \left(\frac{\partial \mathcal{L}}{\partial \dot{x}^\mu} \right) - \frac{\partial \mathcal{L}}{\partial x^\mu} = 0, \quad (11)$$

the two conserved quantities of particle motion that correlate to two Killing vectors can be found as follows

$$\frac{dt}{d\tau} = \dot{t} \equiv u^t = \frac{E}{f(r)}, \quad (12)$$

$$\frac{d\varphi}{d\tau} = \dot{\varphi} \equiv u^\varphi = \frac{L}{r^2}, \quad (13)$$

where the total energy and total angular momentum per unit mass of the particle are denoted by the conserved variables E and L , respectively. Additionally, we may determine $\frac{d\theta}{d\tau} = \dot{\theta} \equiv u^\theta = 0$ using the Euler–Lagrange equation in addition to

$$\frac{dr}{d\tau} = \dot{r} \equiv u^r = \left[-f(r) \left(1 - \frac{E^2}{f(r)} + \frac{L^2}{r^2} \right) \right]^{\frac{1}{2}}. \quad (14)$$

The normalization condition for the test particle’s four-velocity, $u^\mu u_\mu = -1$, and the use of Eqs. (2), (12), and (13) allow one to determine

$$\dot{r}^2 = E^2 - V_{eff}, \quad (15)$$

where the test particle's effective potential, denoted by V_{eff} , can be expressed as follows

$$V_{eff} = f(r) \left(1 + \frac{L^2}{r^2} \right). \quad (16)$$

In the study of geodesic motion, analyzing the effective potential plays a fundamental role. Specifically, the locations of circular orbits correspond to the local extrema of the effective potential. In Fig. 1, the behavior of the effective potential V_{eff} for the loop quantum black hole in comparison to the Schwarzschild ($\gamma = 0$) and RN examples is shown so that Fig. 1a is for $0 < r < 2$ and Fig. 1b is for $r > 2$. As we can see from Fig. 1, the effective potential increases as the value of the parameter γ increases. This is true for the considered ranges of r in Figs. 1a and 1b.

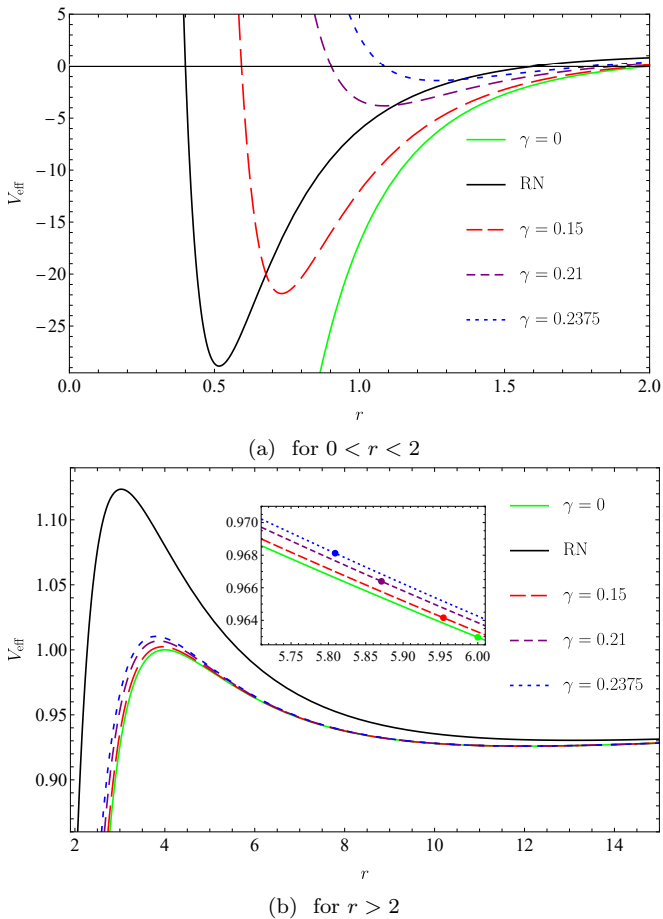


FIG. 1: V_{eff} of the static spherically symmetric loop quantum black hole shown against r for a range of γ values. The Schwarzschild ($\gamma = 0$) and RN solutions are shown by the green and black solid lines, respectively. The colored dots show the locations of ISCOs.

A test particle traveling around the black hole at a fixed radial coordinate r is said to be on a circular orbit. Depending on how the effective potential V_{eff} behaves, circular orbits can be either stable or unstable. Accordingly, the primary feature of circular orbits is $\dot{r} = \ddot{r} = 0$ (or in other words $u^r = \dot{u}^r = 0$). Therefore, it is possible to confirm that for circular orbits, the conditions $E^2 = V_{eff}$ and thus, $\frac{dV_{eff}}{dr} = 0$ must be met using Eqs. (14) and (15). Solving these equations simultaneously, the following relations for the total (specific) energy E , total (specific) angular momentum L , and the angular velocity $\Omega_\varphi \equiv \frac{d\varphi}{dt} = \frac{u^\varphi}{u^t}$ for the test particle in the loop quantum black hole background are obtained by using Eqs. (2), (12), and (13)

$$E^2 = \frac{2f^2(r)}{2f(r) - rf'(r)}, \quad (17)$$

$$L^2 = \frac{r^3 f'(r)}{2f(r) - rf'(r)}, \quad (18)$$

$$\Omega_\varphi^2 = \frac{1}{2r} f'(r), \quad (19)$$

where differentiation with respect to the radial coordinate r is represented by a prime. Eqs. (17)-(19) demonstrate that for unstable circular orbits to exist according to $[(2f(r) - rf'(r)) > 0]$, the total energy and angular momentum must be real.

Figure 2 shows the behaviour of E^2 versus r , indicating that increasing the parameter γ decreases the specific energy of the test particle in the spacetime of the loop quantum black hole, while far from the source, the energy becomes almost constant. This figure depicts the energy for the Schwarzschild and RN solutions. For the Schwarzschild case, it consistently has higher values than the loop quantum black hole case while for the RN case, it is smaller than the loop quantum black hole case.

Figure 3 shows the relationship between L^2 and r for the loop quantum black hole in comparison with the Schwarzschild and the RN solutions in GR for various γ values. An increase in γ results in a decrease in L^2 . Again, for the Schwarzschild case, L^2 values consistently have higher values than the loop quantum black hole case while for the RN case, they are smaller than the loop quantum black hole case.

In Fig. 4, we see the curves of Ω_φ^2 versus r for the loop quantum black hole in comparison with the

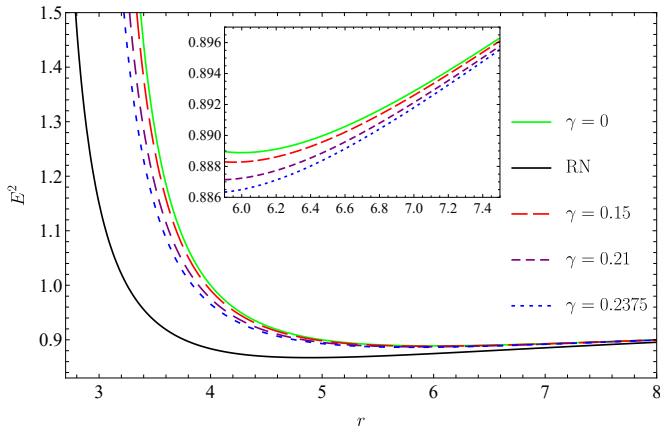


FIG. 2: The plot of E^2 of the static spherically symmetric loop quantum black hole versus r for different values of γ . The green and black solid lines are for the case of Schwarzschild and RN solutions, respectively.

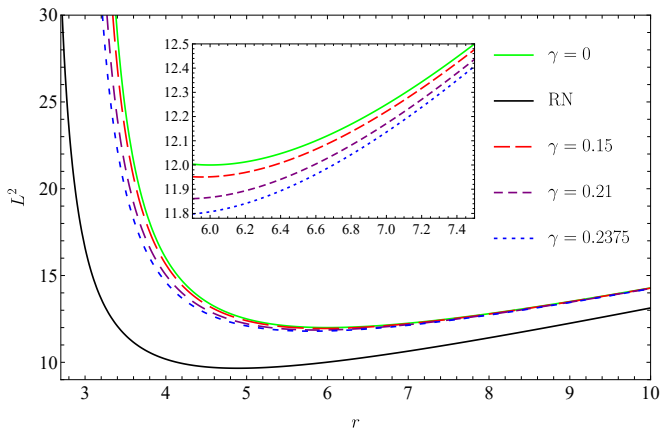


FIG. 3: The behavior of L^2 of the static spherically symmetric loop quantum black hole versus r for various γ values. The green and black solid lines represent the Schwarzschild and RN solution, respectively.

Schwarzschild and RN cases. We see that increasing γ leads to reduction of the value of Ω_φ^2 so that the curve of the Schwarzschild case contains higher values of Ω_φ^2 than the corresponding ones in the loop quantum black hole.

In addition to fulfilling the conditions of circular orbits, a local minimum of V_{eff} is necessary for a stable circular orbit, hence its second derivative needs to be positive as $\frac{d^2V_{eff}}{dr^2} > 0$ for a stable circular orbit. On the other hand, an unstable circular orbit occurs at a local maximum, meaning $\frac{d^2V_{eff}}{dr^2} < 0$. The boundary (transition) between stable and unstable circular orbits is defined by the innermost (marginally) stable circular orbit (ISCO).

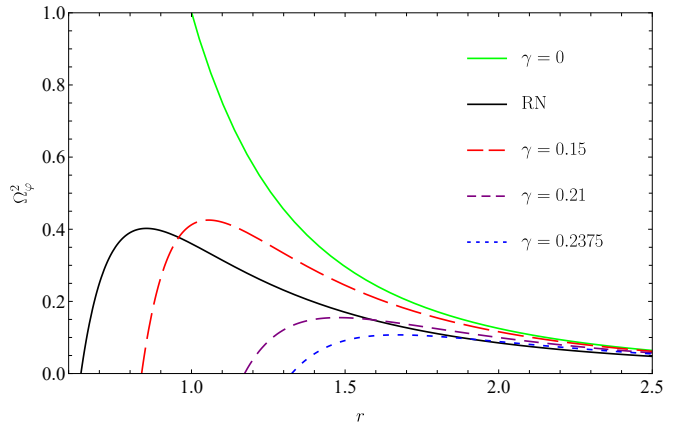


FIG. 4: The plot of Ω_φ^2 of the static spherically symmetric loop quantum black hole versus r for various γ values. The green and black solid lines represent the Schwarzschild and RN solutions, respectively.

The effective potential at this critical radius satisfies

$$\frac{dV_{eff}}{dr} = 0, \quad \frac{d^2V_{eff}}{dr^2} = 0, \quad (20)$$

simultaneously. ISCO's existence, r_{ISCO} , is entirely a relativistic occurrence. In contrast to classical mechanics, where the effective potential has only one minimum, in general relativity, depending on the choice of L , the effective potential can produce either a local maximum and minimum or no extremum. This extremum is associated with a stable outer and an unstable inner circular orbit for the test particle. For a given value of L , ISCO is the point at which the stable and unstable circular orbits intersect. The explicit analytical form of ISCO associated with the loop quantum black hole can not be available. Therefore, one can numerically solve the equation set (20) to yield the values of the ISCO for the test particle moving in the spacetime of the loop quantum black hole. Next, we obtain the numerical values of r_{ISCO} , L_{ISCO} , and E_{ISCO} for the static spherically symmetric loop quantum black hole for three distinct values of the loop quantum gravity parameter γ in Table I. The ISCO for the Schwarzschild and RN black holes, on the other hand, are $6M$ and $5.4M$. The ISCO associated with the loop quantum black hole therefore decreases as the value of γ increases, as Table I shows.

Using Eqs. (13) and (15), one can find the relation between r and φ in the spacetime of this loop quantum

TABLE I: The numerical values of r_{ISCO} , L_{ISCO} , and E_{ISCO} for a test particle moving in the loop quantum black hole spacetime associated with different values of γ . (We have set $M = 1$)

ISCO Parameters			
γ	r_{ISCO}	E_{ISCO}	L_{ISCO}
0	6	0.94280	3.4641
0.15	5.95435	0.942482	3.45694
0.21	5.87075	0.942206	3.44394
0.2375	5.80859	0.941893	3.4344

black hole as follows

$$\left(\frac{dr}{d\varphi}\right)^2 = \frac{r^4}{L^2} \left(E^2 - f(r) \left(1 + \frac{L^2}{r^2} \right) \right). \quad (21)$$

By numerically solving Eq. (21) and plotting the solutions on the Cartesian coordinates, the trajectories of the test particle around the loop quantum black hole can be gathered as shown in Fig. 5. Indeed, Fig. 5 shows the

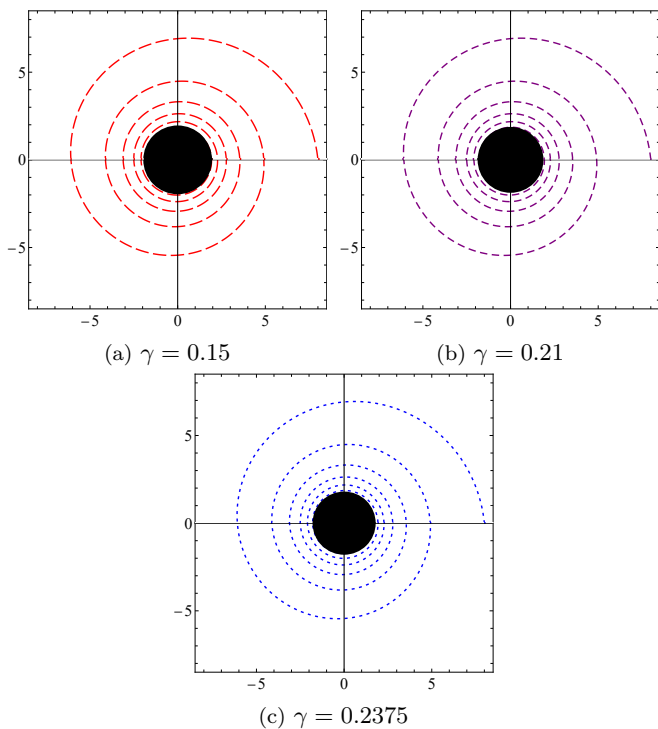


FIG. 5: The trajectories of the test particle in the vicinity of the loop quantum black hole inspired by LQG for various values of γ .

trajectory of the test particle for different values of the LQG parameter. As shown in Fig. 5, the trajectories of

the test particle appear nearly identical despite variations in γ . This is because the selected γ values are close to each other and relatively small, resulting in only a minor contribution from the γ^3 term in the black hole metric. Consequently, the effect of γ on the particle's trajectory remains negligible within this parameter space.

IV. THE MOTION OF ELECTRICALLY CHARGED PARTICLES

Energy and angular momentum can be transferred from the black hole to the accretion disk if a magnetic coupling process is present in the neighborhood of a loop quantum black hole [43–47]. Consequently, the magnetic field intensity on the black holes's horizon is given as [42]

$$B_h = \frac{1}{r_+} \sqrt{2m_p \dot{M} c}, \quad (22)$$

where c is the speed of light, m_p is the magnetization parameter, and the index (h) is the abbreviation for horizon. Also, $m_p = 1$ denotes the equipartition state for the accretion and magnetic coupling process. Black holes and other compact objects can have magnetic fields around them, according to both theoretical and experimental evidence [48–51]. Here, we assume that the background geometry is unaffected by the energy of a weak magnetic field [52]. Weakly magnetized is the term used to describe this kind of loop quantum black hole. Furthermore, we assume that the magnetic field around the black hole is static, axisymmetric, and homogeneous at spatial infinity, where it has the strength B . The presence of such a magnetic field is necessary for studying the motion of an electrically charged test particle with mass m and electric charge q around the loop quantum black hole.

In accordance with the methodology presented in Refs. [42, 47, 50], our objective is to compute the magnetic field surrounding the loop quantum black hole. In this setup, according to the above assumptions, we take into account the following Wald-like electromagnetic 4-potential (see Appendix A for more details)

$$A_\mu = \left(0, 0, 0, \frac{B}{2} \left(r^2 + \frac{\alpha}{r^2} \right) \sin^2 \theta \right), \quad (23)$$

which approximately satisfies the covariant Maxwell's equations up to first order in α . Additionally, the magnetic field as observed by a local observer with 4-velocity

w_μ can be defined as follows

$$\mathcal{B}^\mu = -\frac{\epsilon^{\mu\nu\lambda\sigma}}{\sqrt{-\bar{g}}} F_{\lambda\sigma} w_\nu, \quad (24)$$

where $\bar{g} = g_{tt}g_{rr}g_{\theta\theta}g_{\varphi\varphi}$ is the metric determinant of the loop quantum black hole described in Eq. (2), $F_{\mu\nu} = \partial_\mu A_\nu - \partial_\nu A_\mu$ is the electromagnetic field tensor, and $\epsilon^{\mu\nu\lambda\sigma}$ is the Levi-Civita symbol. The 4-velocity of the observer can be written as follows to satisfy the forward-in-time condition

$$w_\mu = \left(\frac{1}{\sqrt{f(r)}}, 0, 0, 0 \right). \quad (25)$$

Therefore, the magnetic field can be obtained by using Eqs. (23)-(25)

$$\begin{aligned} \mathcal{B}^\mu &= \frac{B}{\sqrt{f(r)}} \\ &\times \left(0, \left(1 + \frac{\alpha}{r^4}\right) \cos\theta, -\left(1 - \frac{\alpha}{r^4}\right) \frac{\sin\theta}{r}, 0 \right), \end{aligned} \quad (26)$$

in which clearly its r - and θ -components are non-zero. At spatial infinity, it is assumed that the magnetic field moves upward along the z -axis [53].

The electrically charged test particle moving in the spacetime of the loop quantum black hole has the following Lagrangian

$$\tilde{\mathcal{L}} = \frac{1}{2} g_{\mu\nu} \dot{x}^\mu \dot{x}^\nu + \frac{q}{m} A_\mu \dot{x}^\mu. \quad (27)$$

Just like in the last section, we use the Euler-Lagrange equation (11) at the equatorial plane to find

$$\dot{t} \equiv \tilde{u}^t = \frac{\tilde{E}}{f(r)}, \quad (28)$$

and

$$\dot{\varphi} \equiv \tilde{u}^\varphi = \frac{\tilde{L}}{r^2} - \frac{qB}{2m} \left(1 + \frac{\alpha}{r^4}\right), \quad (29)$$

where the electrically charged test particle's four-velocity is \tilde{u}^μ , and its specific energy and specific angular momentum are \tilde{E} and \tilde{L} , respectively. Once more, the normalizing condition $\tilde{u}^\mu \tilde{u}_\mu = -1$ can be used on the equatorial plane to obtain

$$\dot{r}^2 = \tilde{E}^2 - \tilde{V}_{eff}, \quad (30)$$

where \tilde{V}_{eff} is the effective potential felt by the electrically charged test particle, which is defined as

$$\tilde{V}_{eff} = f(r) \left(1 + r^2 \left(\frac{\tilde{L}}{r^2} - \frac{qB}{2m} \left(1 + \frac{\alpha}{r^4}\right) \right)^2 \right). \quad (31)$$

The plot of \tilde{V}_{eff} versus r for the electrically charged test particle traveling in the spacetime of the loop quantum black hole for various values of γ is shown in Fig. 6. As we can see from this figure, increasing γ raises the effective potential values.

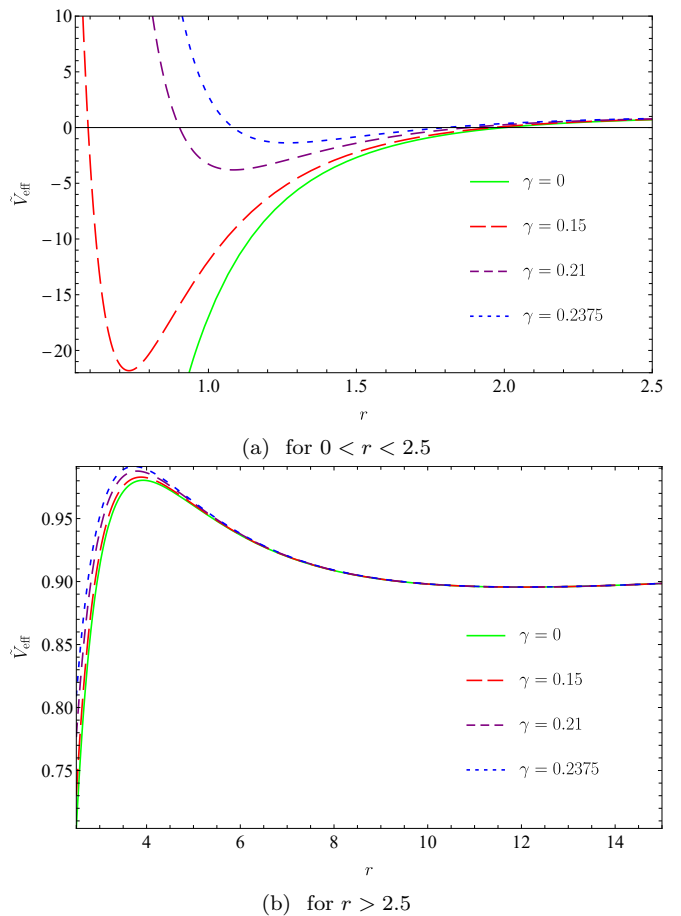


FIG. 6: The effective potential \tilde{V}_{eff} felt by the massive electrically charged test particle moving in the static spherically symmetric loop quantum black hole's spacetime as a function of r for various γ values. The Schwarzschild solution situation in GR is shown by the green solid line.

As in the previous section, circular orbits require that $\tilde{E}^2 = \tilde{V}_{eff}$ and $\frac{d\tilde{V}_{eff}}{dr} = 0$ be met. Thus, Eqs. (2), (28), and (29) are used to solve these equations simultaneously and produce the following relations

$$\tilde{E} = \sqrt{f(r) + \frac{f(r) [Bqf(r) (r^4 - \alpha) + y_1]^2}{m^2 r^6 (rf'(r) - 2f(r))^2}}, \quad (32)$$

$$\tilde{L} = \frac{Bqr (\alpha + r^4) f'(r) - 4\alpha Bqf(r) - 2y_1}{2mr^2 y_2}, \quad (33)$$

$$\tilde{\Omega}_\varphi = \frac{f(r)}{\tilde{E}} \left(\frac{\tilde{L}}{r^2} - \frac{qB}{2m} \left(1 + \frac{\alpha}{r^4} \right) \right), \quad (34)$$

where we have defined

$$y_1 = \left((Bqf(r))^2 (r^4 - \alpha)^2 - m^2 r^8 (f'(r))^2 + 2m^2 r^7 f(r) f'(r) \right)^{\frac{1}{2}}, \quad (35)$$

and

$$y_2 = r f'(r) - 2f(r). \quad (36)$$

The massive electrically charged test particle moving in a loop quantum black hole spacetime has an ISCO location that satisfies the requirements (20). As we previously stated, the complexity of the metric coefficient (2) prevents the availability of the explicit analytical form of ISCO for the electrically charged test particle moving in the loop quantum black hole spacetime. The numerical values of the ISCO for the electrically charged test particle moving in the spacetime of the loop quantum black hole can therefore be obtained by numerically solving the equations set (20). This can be done in Table II, by collecting numerical values of \tilde{r}_{ISCO} , \tilde{L}_{ISCO} , and \tilde{E}_{ISCO} for various values of γ that correspond with the electrically charged test particle for the static spherically symmetric loop quantum black hole. Table II shows that the ISCO radius of the electrically charged test particle connected with the loop quantum black hole decreases as γ increases. By comparing Tables I and II, we can see that the ISCO values associated with the loop quantum black hole that is weakly magnetized, are smaller than those associated with the normal loop quantum black hole.

TABLE II: For an electrically charged test particle moving in the static spherically symmetric loop quantum black hole spacetime, the numerical values of \tilde{r}_{ISCO} , \tilde{L}_{ISCO} , and \tilde{E}_{ISCO} correspond to various values of γ are collected. (We have set $M = 1$)

ISCO Parameters			
γ	\tilde{r}_{ISCO}	\tilde{E}_{ISCO}	\tilde{L}_{ISCO}
0	5.95709	0.96014	3.41232
0.15	5.91275	0.95975	3.40531
0.21	5.83151	0.95905	3.39261
0.2375	5.77105	0.95851	3.38328

V. NOVIKOV–THORNE MODEL OF THE ACCRETION DISK: NEUTRAL PARTICLES

Black hole accretion disks are essential to astrophysical processes because they are the main sources of electromagnetic radiation emission and mass-energy transfer. A strong relativistic framework for explaining the dynamics and radiative characteristics of geometrically thin, optically thick disks in the vicinity of the loop quantum black hole is offered by the Novikov–Thorne model [54], one of the several accretion disk models. By adding broad relativistic effects, this model expands on the traditional Shakura–Sunyaev [55] prescription and plays a crucial role in comprehending the observational signs of black hole accretion. A thin accretion disk is defined by a vertical scale height h that is much smaller than its radial extension r , i.e., $h \ll r$. This characteristic of the thin accretion disk created in the loop quantum black hole's surrounding environment results in negligible vertical pressure and entropy gradients within the disk. As a result, the disk is predominantly influenced by hydrodynamic equilibrium. The accretion disk remains effectively cool due to the emission of thermal radiation from its surface, preventing any buildup of heat generated by internal stresses and dynamical friction. As a result, the plasma is able to spiral inward along stable, nearly circular paths governed by Keplerian dynamics. This leads to the development of a stable, thin disk structure, whose inner boundary lies at a stable orbit near the black hole.

The bolometric luminosity of the accretion disk can be defined as [56, 57]

$$\mathcal{L}_{bol} = \eta \dot{M} c^2, \quad (37)$$

Here, \dot{M} denotes the mass accretion rate onto the black hole, while η signifies the energy conversion efficiency of the accretion disk. From an astrophysical standpoint, directly measuring the bolometric luminosity presents significant difficulties, which vary depending on the characteristics and classification of the black hole. Therefore, theoretical frameworks and modeling approaches are essential for estimating the bolometric luminosity. A key aspect of such analyses is determining the efficiency of the accretion disk, which reflects the maximum amount of energy extractable from the inflowing matter before it crosses the event horizon. This efficiency is vital in

describing the accretion dynamics, as the infalling material's rest mass is partially converted into electromagnetic radiation near the core. The rate of this radiation, particularly from photons escaping the disk surface, provides a basis for calculating the energy efficiency [54, 58]. Specifically, by evaluating the energy of particles at the innermost stable circular orbit (ISCO), one can assess the efficiency under the assumption that emitted photons reach distant observers without being captured by the black hole [59, 60].

$$\eta = 1 - E_{ISCO}. \quad (38)$$

The radiative efficiency η of photons emitted from the accretion disk can be determined by evaluating the energy observed at the ISCO, as previously described. Utilizing the dataset provided in Table I, we analyze the energy efficiency of the accretion disk in the context of a loop quantum black hole. The computed efficiency values are listed in Table III. The findings indicate that radiative efficiency increases with higher values of the parameter γ . Notably, the Schwarzschild black hole emerges as a special case when $\gamma = 0$, where the corresponding efficiency is approximately $\eta \approx 5.72\%$ (see also Ref. [61]). For a Reissner–Nordström (RN) black hole, the radiative efficiency is estimated to be around $\eta \approx 7.5\%$.

TABLE III: Value of the radiative efficiency of the accretion disk of the loop quantum black hole arranged for the different values of parameter γ . (We have set $M = 1$)

Radiative efficiency		
γ	r_{ISCO}	$\eta\%$
0	6	5.72%
0.15	5.95435	5.75%
0.21	5.87075	5.77%
0.2375	5.80859	5.81%

A. Thin accretion disk properties

In this section, we explore the radiation flux emitted by the accretion disk surrounding a loop quantum black hole. Accretion disks typically consist of gas and dust particles orbiting in stable paths around compact objects such as black holes or neutron stars. As these materials

revolve around the central mass, the curvature of space-time can cause them to gradually lose both energy and angular momentum. This loss drives the gas and dust inward, drawing them closer to the inner edge of the disk and eventually toward the compact object. During this inward spiral, the material heats up due to friction and other dissipative processes, emitting radiation in the process—this is the origin of accretion disk luminosity. In the context of loop quantum gravity, it is expected that the specific parameters of the loop quantum black hole influence the behavior and radiation characteristics of the accreting matter. The presence of the loop quantum parameter, in particular, could significantly affect the dynamics and emission properties of the disk. Therefore, studying the radiation flux in this setting not only helps in understanding key physical features of accretion disks but also holds potential for observable signatures that could serve as tests for loop quantum gravity effects. The electromagnetic radiation flux can be described by the following relation [54, 55, 62]:

$$\mathcal{F}(r) = \frac{-\dot{M}}{4\pi\sqrt{-g}} \frac{\Omega_{,r}}{(E - \Omega L)^2} \int_{r_{ISCO}}^r (E - \Omega L) L_{,r} dr, \quad (39)$$

where the determinant of three-dimensional subspace is given as $g = g_{tt}g_{rr}g_{\varphi\varphi}$.

Here, we suppose that the loop quantum black hole has a total mass of $M = 2.5 \times 10^6 M_{\odot}$ and an accretion rate of $\dot{M} = 2 \times 10^{-6} M_{\odot} yr^{-1}$ to analyze the flux distribution of its accretion disk. One can express the rate in terms of the Eddington accretion rate to find $\dot{M} = 3.63 \times 10^{-4} \dot{M}_{Edd}$, which is within the typical range for supermassive black holes.

The Eddington luminosity represents the maximum energy output an object can achieve when the outward radiation pressure precisely counteracts the inward gravitational pull. Therefore, the Eddington luminosity is given by

$$\mathcal{L}_{Edd} = 1.26 \times 10^{38} \left(\frac{M}{M_{\odot}} \right) \text{ erg/s}, \quad (40)$$

and for an accreting black hole, the Eddington mass accretion rate is defined through the relation [63]

$$\dot{M}_{Edd} = \frac{\mathcal{L}_{Edd}}{\eta c^2}. \quad (41)$$

For a geometrically thin accretion disk with its inner boundary at the ISCO radius, the accretion luminosity

typically falls between 5% and 30% of the Eddington limit [64–67]. Based on this, the chosen values of M and \dot{M} remain below the Eddington threshold while characterizing a supermassive black hole. A well-known example is the Sgr A* supermassive black hole, located at the center of the Milky Way, which has an estimated mass of $M = 4.1 \times 10^6 M_\odot$ and an accretion rate in the range $\dot{M} \sim 10^{-9} - 10^{-7} M_\odot \text{ yr}^{-1}$ [68].

Eqs. (17)–(19) are also used to further determine the electromagnetic radiation flux. However, it turns out that obtaining the analytical expression of the flow is difficult, thus we use a numerical method, refer to Fig. 7. Figure 7 shows that the electromagnetic radiation flux approaches bigger values when the γ parameter is increasing. We present the electromagnetic radiation flux for the Schwarzschild and RN black hole cases for a better comparison, in Fig. 7.

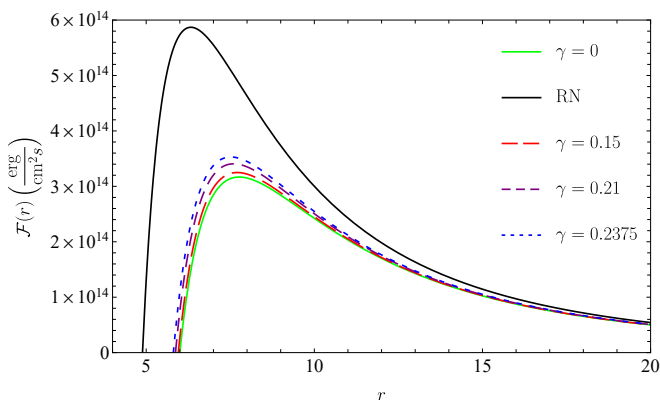


FIG. 7: The illustration of the radial dependence of accretion disk’s electromagnetic radiation flux of the loop quantum black hole as the Sgr A* supermassive black hole with $\dot{M} = 10^{-7} M_\odot \text{ yr}^{-1}$ for various values of γ . The green solid and black solid curves are associated with the Schwarzschild and RN black hole cases, respectively.

As previously described, the Novikov–Thorne model assumes the accreted matter is in thermodynamic equilibrium. This assumption suggests that the disk’s radiation can be regarded as ideal black body radiation. Therefore, the energy flux $\mathcal{F}(r)$ and the local effective temperature on the disk T_{eff} are related together according to the Stefan-Boltzmann law as follows

$$\mathcal{F}(r) = \sigma_{SB} T_{eff}^4, \quad (42)$$

where $\sigma_{SB} = 5.67 \times 10^{-5} \text{ erg} \cdot \text{cm}^{-2} \cdot \text{s}^{-1} \cdot \text{K}^{-4}$ is the Stefan–Boltzmann constant. Fig. 8 illustrates the radial

dependency of the local effective temperature on the accretion disk of the loop quantum black hole for different values of γ . As can be observed from Fig. 8, similarly the local effective temperature on the accretion disk of the loop quantum black hole rises with increasing loop quantum parameter γ . Also, in Fig. 8, the local effective temperature on the accretion disk of the Schwarzschild and RN black hole cases are also depicted for a better comparison.

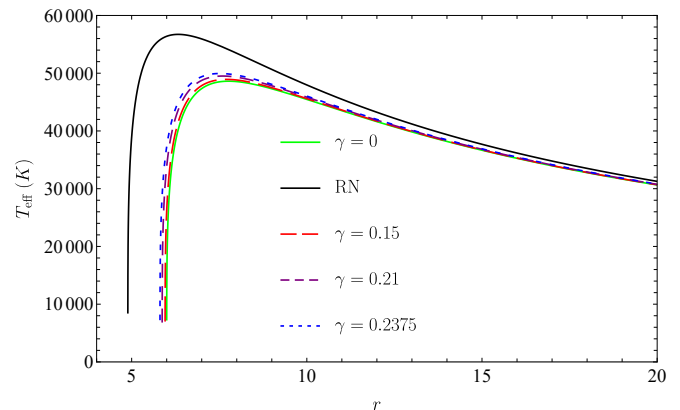


FIG. 8: The illustration of the radial dependence of accretion disk’s local effective temperature of the loop quantum black hole as the Sgr A* supermassive black hole with $\dot{M} = 10^{-7} M_\odot \text{ yr}^{-1}$ for various values of γ . The green solid and black solid curves are associated with the Schwarzschild and RN black hole cases, respectively.

In Fig. 9, we display a density plot of the accretion disk’s local effective temperature for more detail. Figure 9 shows how the disk’s local effective temperature changes when the loop quantum correction parameter varies. Notably, this density plot demonstrates that the accretion disk’s local effective temperature is sufficiently heated, particularly near the black hole, but then it begins to cool toward its outer edge.

The differential luminosity that a distant observer receives at infinity is another important parameter we will discuss. It can be expressed as [54, 55, 62]

$$\frac{d\mathcal{L}_\infty}{d \ln r} = 4\pi r \sqrt{-g} E \mathcal{F}(r). \quad (43)$$

We analyze the differential luminosity profile of the accretion disk and present its radial distribution in Fig. 10. In line with the behavior observed for the accretion flux, an increase in the loop quantum parameter γ leads to a corresponding rise in differential luminosity. Notably, the

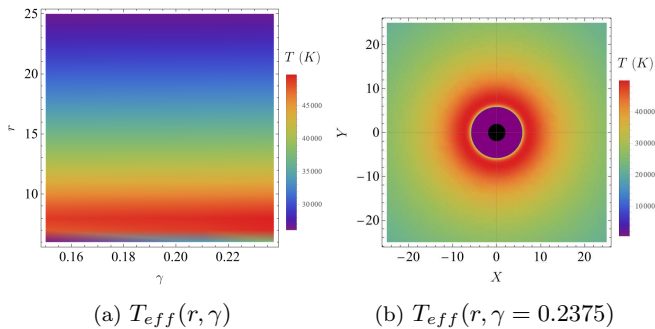


FIG. 9: (a): The local effective temperature profile of the loop quantum black hole parameter in terms of r and γ in the form of a density plot. (b): The local effective temperature profile on the equatorial plane of $X - Y$ Cartesian coordinates in the form of a density plot.

luminosity decreases with radial distance from the black hole, highlighting that the influence of γ is most pronounced in the immediate vicinity of the event horizon. Through detailed examination, our findings suggest that the presence of the loop quantum correction parameter γ enables the accretion disk to retain radiative energy more effectively and may suppress electromagnetic emission at its surface.

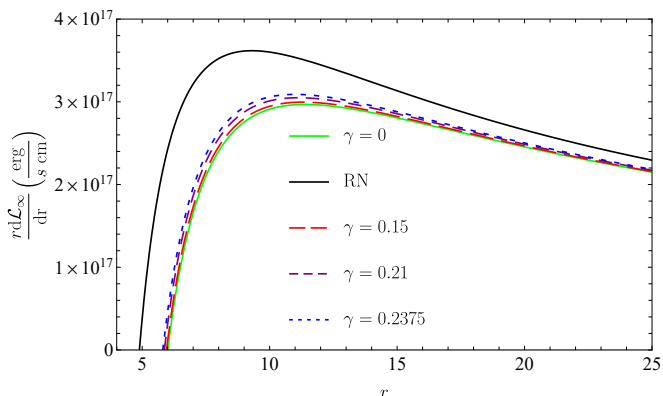


FIG. 10: The illustration of the radial dependence of accretion disk's differential luminosity received by an observer far from the loop quantum black hole as the Sgr A* supermassive black hole with $\dot{M} = 10^{-7} M_\odot \text{ yr}^{-1}$ for various values of γ . The green solid and black solid curves are related to the Schwarzschild and RN black hole cases, respectively.

The change in frequency of a photon as it moves from the source of emission to the observer— that is, its redshifted blackbody spectrum— is associated with the observed luminosity \mathcal{L}_∞ of the thin accretion disk around

the loop quantum black hole [69–72]. Therefore, the spectral luminosity \mathcal{L}_∞ received by a distant observer is as follows

$$\mathcal{L}_\infty = \frac{8\pi h \cos \psi}{c^2} \int_{r_i}^{r_f} \int_0^{2\pi} \frac{\nu_e^3 r dr d\varphi}{\exp\left[\frac{h\nu_e}{k_B T_{eff}}\right] - 1}, \quad (44)$$

where h denotes the Planck constant, k_B stands for the Boltzmann constant, ψ signifies the inclination angle of the accretion disk, and r_i and r_f correspond to the inner and outer radii of the disk surrounding the loop quantum black hole. Furthermore, the emitted photon frequency ν_e undergoes redshift to

$$\nu = \frac{\nu_e}{(1+z)}, \quad (45)$$

where ν represents the photon frequency as perceived by a distant observer. Accounting for both gravitational redshift and the Doppler effect, the redshift factor is given by

$$(1+z) = \frac{1 + \Omega r \sin \varphi \sin \psi}{\sqrt{-g_{tt} - g_{\varphi\varphi} \Omega^2}}, \quad (46)$$

and assuming negligible light bending, which may hold as a reasonable approximation for small inclination angles ψ , the temperature measured by a remote observer is expressed as [69, 72]

$$T_\infty = \frac{T_{eff}}{(1+z)}. \quad (47)$$

Additionally, \mathcal{L}_∞ can also represent as the thermal energy flux radiated by the accretion disk encircling the loop quantum black hole.

To plot the spectral luminosity \mathcal{L}_∞ of the accretion disk around the loop quantum black hole, we consider $r_i = r_{ISCO}$ and $r_f = \infty$, as the flux across the disk surface diminishes when $r \rightarrow \infty$ in the case of the loop quantum black hole, and also we set $\psi = 0$. As a point of note, we used $r_f = 100$ for simplicity since it is less time-consuming than $r_f = \infty$ but does not make much difference in the result. Figure 11 shows the spectral luminosity received by an observer far from the loop quantum black hole. Similar to the differential flux and temperature, from Fig. 11, we see that increasing the loop quantum parameter γ leads to amplification of the spectral luminosity. The spectrum appears to be a blackbody distribution, with a peak at higher frequencies. When the

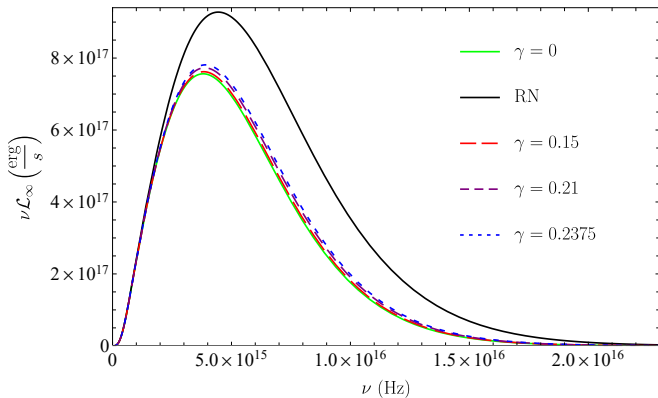


FIG. 11: *The illustration of the radial dependence of accretion disk's spectral luminosity received by an observer far from the loop quantum black hole as the Sgr A* supermassive black hole with $\dot{M} = 10^{-7} M_{\odot} \text{ yr}^{-1}$ for various values of γ . The green solid and black solid curves are related to the Schwarzschild and RN black hole cases, respectively.*

frequency is low, however, we cannot distinguish between different cases corresponding to each γ .

Before presenting our final conclusions, it is important to note that the quantum effects in this loop quantum black hole spacetime are governed by the intrinsic Barbero–Immirzi parameter and the minimum mass, raising an intriguing question regarding the potential observational signatures of these effects. Identifying such signatures in current or upcoming experiments could provide a means to directly test or constrain quantum gravitational effects. Over the past decades, extensive studies have explored this possibility using various experimental and observational approaches [73–80]. However, these studies have primarily focused on the classical region outside the black hole horizon, where quantum gravitational effects remain exceedingly small. In this work, we consider a quantum extension of black hole spacetime in which the classical singularity is resolved, leading to quantum effects extending into the exterior region (see also [31]). Given this framework, it is of particular interest to investigate how these quantum effects influence the properties of accretion disks, potentially offering new observational avenues to probe quantum gravity. On the other hand, it is important to note that the effects of loop quantum gravity on astrophysical black holes are generally expected to be extremely small. Consequently, the results obtained in this study are most relevant for small-

mass black holes, such as micro-black holes, TeV-scale black holes, and potentially primordial black holes. The significance of this study lies in the unique intersection of astrophysics, particle physics, and quantum gravity that the analysis of accretion disks around quantum or small-mass black holes provides. This framework offers a means to test fundamental phenomena such as Hawking radiation and black hole evaporation, place constraints on primordial black holes as dark matter candidates, identify potential observational signatures of quantum gravity effects, and explore physics beyond the Standard Model. Additionally, we note that a similar quantum (string)-corrected black hole solution has been reported in Ref. [81]. Both metrics exhibit a $\frac{1}{r^4}$ decay due to quantum corrections. In comparison, the Barbero–Immirzi parameter γ in our model plays an analogous role to the parameter λ introduced in the aforementioned reference.

VI. CONCLUSIONS

In this study, we investigated motion of neutral and electrically charged particles, circular orbits and radiation properties of the accretion disk around the loop quantum black hole, as accretion disk radiation can be influenced by LQG parameter. The theoretical study of accretion disk radiation around a loop quantum black hole is considered to be a powerful test of its useful properties and astrophysical observations. We discovered that increasing the parameter γ increases the effective potential of neutral particles in the loop quantum black hole, exactly the same for electrically charged particles far away from the source. Furthermore, we found that increasing the parameter γ in the LQG black hole model decreases the neutral test particle's specific energy, angular momentum and its angular velocity. To investigate the dynamics of electrically charged particles in the vicinity of a loop quantum black hole, we consider a background magnetic field that is static, axisymmetric, and asymptotically homogeneous. Within this framework, a Wald-like electromagnetic four-potential is employed, which includes the quantum corrections introduced by LQG. This potential approximately satisfies the covariant Maxwell's equations up to first order in the loop quantum parameter α . Furthermore, we analyzed the effective potential ex-

perienced by the charged test particle and computed the numerical values of the ISCO radii for the charged particles around the loop quantum black hole spacetime. Our findings indicate that increasing loop quantum parameter diminish the ISCO radius of test particles, whether neutral or charged. Further, we investigated radiative efficiency and presented our findings in Table III. Radiative efficiency rises as loop quantum parameter γ grows.

Finally, we considered the accretion disk around the black hole as a primary source of information associated with the surrounding spacetime geometry and its nature in LQG. To provide valuable insights into the unique properties of the deformed Schwarzschild black hole inspired by LQG, we studied the influence of the loop quantum correction parameter on the accretion disk radiative properties, such as the flux of electromagnetic radiation, the temperature, differential luminosity, and the spectral luminosity of the disk. As a result the luminosity spectrum exhibits a blackbody-like distribution, characterized by a peak at higher frequencies. However, in the low-frequency regime, the spectral profiles corresponding to different values of γ become nearly indistinguishable, making it difficult to differentiate between them. Interestingly, we found that the curves of these accretion disk radiation quantities shift upwards toward their bigger values as a result of the rise in the value of the loop quantum correction parameter α , resulting in these quantities decreasing compared to the Schwarzschild and RN black hole cases in Einstein gravity. Based on the obtained results, it was observed that the accretion disk around the loop quantum black hole can retain the radiative energy to prevent the electromagnetic radiation from emitting on the disk surface as a consequence of the influence of the loop quantum correction parameter α .

ACKNOWLEDGMENTS

The Work of K. Nozari and S. Saghafi is supported financially by the INSF of Iran under the grant number 4038520. The authors want to express their gratitude to the respected referee for carefully reading the manuscript and the insightful comments, which significantly improved the quality of the manuscript.

Appendix A: Derivation of Electromagnetic 4-Potential

Inspired by Wald's solution [82], we write the following general ansatz for the electromagnetic 4-potential

$$A_\mu = \left(0, 0, 0, \frac{B}{2} \Psi(r) \sin^2 \theta \right), \quad (\text{A1})$$

where B is the strength of the weak magnetic field, and $\Psi(r)$ is an unknown function of r , which we want to determine it such that Maxwell's equations are satisfied. The Maxwell's equations in curved spacetime without possible sources are as follows

$$\nabla_\mu F^{\mu\nu} = \frac{1}{\sqrt{-\bar{g}}} \partial_\mu (\sqrt{-\bar{g}} F^{\mu\nu}) = 0, \quad (\text{A2})$$

where $\sqrt{-\bar{g}} = r^2 \sin \theta$ in which $\bar{g} = g_{tt} g_{rr} g_{\theta\theta} g_{\varphi\varphi}$ is the metric determinant of the loop quantum black hole described in Eq. (2), and $F_{\mu\nu} = \partial_\mu A_\nu - \partial_\nu A_\mu$ is the electromagnetic field tensor. Using the ansatz (A1), the non-zero components of $F_{\mu\nu}$ can be found as follows

$$\begin{aligned} F_{r\varphi} &= \partial_r A_\varphi = \frac{B}{2} \Psi'(r) \sin^2 \theta = -F_{\varphi r}, \\ F_{\theta\varphi} &= \partial_\theta A_\varphi = B \Psi(r) \sin \theta \cos \theta = -F_{\varphi\theta}, \end{aligned} \quad (\text{A3})$$

where a prime stands for a derivative with respect to the radial coordinate r . It should be noted that the components of the inverse of electromagnetic field tensor through the relation $F^{\mu\nu} = g^{\mu\alpha} g^{\nu\beta} F_{\alpha\beta}$ are as follows

$$\begin{aligned} F^{r\varphi} &= g^{rr} g^{\varphi\varphi} F_{r\varphi} = \frac{B}{2r^2} f(r) \Psi'(r), \\ F^{\theta\varphi} &= g^{\theta\theta} g^{\varphi\varphi} F_{\theta\varphi} = \frac{B}{r^4} \Psi(r) \tan \theta. \end{aligned} \quad (\text{A4})$$

Inserting (A4) into the Maxwell's equations (A2) leads to the following expression

$$\nabla_\mu F^{\mu\nu} = \frac{B}{r^2} \left(\frac{1}{2} (f(r) \Psi'(r))' - \frac{1}{r^2} \Psi(r) \right) = 0. \quad (\text{A5})$$

As a result of rearranging Eq. (A5), we obtain the primary condition required to satisfy Maxwell's equations by the considered ansatz for the electromagnetic 4-potential

$$(f(r) \Psi'(r))' = \frac{2}{r^2} \Psi(r). \quad (\text{A6})$$

Let's consider the following assumption

$$\Psi(r) = r^2 + \frac{\alpha}{r^2}. \quad (\text{A7})$$

This assumption is quite elegant; it reduces to the standard Wald-type solution when $\alpha \rightarrow 0$ and introduces a correction that is proportional to $1/r^2$, as expected from quantum corrections. By taking into account the assumption (A7), the left-hand side of the primary condition (A6) becomes

$$1 + \frac{3\alpha}{r^4} - \frac{3\alpha M^2}{r^4} - \frac{8\alpha M}{r^5} + \frac{7\alpha^2 M^2}{r^8},$$

while the right-hand side of the primary condition (A6) becomes

$$1 + \frac{\alpha}{r^4}.$$

Thus, this ansatz meets the covariant Maxwell's equations up to $\mathcal{O}(\alpha)$, indicating consistency with minor quantum corrections from LQG, though it does not fully satisfy Maxwell's equations. Consequently, we take into account the Wald-like electromagnetic 4-potential

$$A_\mu = \left(0, 0, 0, \frac{B}{2} \left(r^2 + \frac{\alpha}{r^2} \right) \sin^2 \theta \right), \quad (\text{A8})$$

which approximately satisfies the covariant Maxwell's equations up to $\mathcal{O}(\alpha)$.

-
- [1] B. P. Abbott *et al.*, Phys. Rev. Lett. **116**, 061102 (2016).
[2] B. P. Abbott *et al.*, Phys. Rev. Lett. **116**, 241103 (2016).
[3] K. Akiyama *et al.*, Astrophys. J. Lett. **875**, L1 (2019).
[4] K. Akiyama *et al.*, Astrophys. J. Lett. **875**, L4 (2019).
[5] J. Frank, A. King, and D. Raine, *Accretion Power in Astrophysics* (Cambridge University Press, 2002).
[6] F. Yuan and R. Narayan, Ann. Rev. Astron. Astrophys. **52**, 529 (2014).
[7] S. Nampalliwar and C. Bambi, arXiv e-prints, arXiv:1810.07041 (2018), [arXiv:1810.07041](https://arxiv.org/abs/1810.07041) [astro-ph.HE].
[8] C. Rovelli and L. Smolin, Nuclear Physics B **442**, 593 (1995).
[9] A. Ashtekar and J. Lewandowski, arXiv preprint gr-qc/9711031 (1997).
[10] A. Ashtekar, T. Pawłowski, and P. Singh, Physical Review D—Particles, Fields, Gravitation, and Cosmology **74**, 084003 (2006).
[11] M. Han, Y. Ma, and W. Huang, International Journal of Modern Physics D **16**, 1397 (2007).
[12] A. Ashtekar and P. Singh, Classical and Quantum Gravity **28**, 213001 (2011).
[13] C. Zhang, S. Song, and M. Han, Physical Review D **105**, 064008 (2022).
[14] C. Zhang, H. Liu, and M. Han, Classical and Quantum Gravity **40**, 205022 (2023).
[15] D.-W. Chiou, Physical Review D **78**, 064040 (2008).
[16] R. Gambini and J. Pullin, Physical Review Letters **101**, 161301 (2008).
[17] H. M. Haggard and C. Rovelli, Physical Review D **92**, 104020 (2015).
[18] M. Christodoulou, C. Rovelli, S. Speziale, and I. Vilenky, Physical Review D **94**, 084035 (2016).
[19] A. Ashtekar, J. Olmedo, and P. Singh, Physical Review Letters **121**, 241301 (2018).
[20] C. Zhang, Y. Ma, S. Song, and X. Zhang, Physical Review D **102**, 041502 (2020).
[21] C. Zhang, Y. Ma, S. Song, and X. Zhang, Physical Review D **105**, 024069 (2022).
[22] J. Lewandowski, Y. Ma, J. Yang, and C. Zhang, Physical Review Letters **130**, 101501 (2023).
[23] V. Husain, J. G. Kelly, R. Santacruz, and E. Wilson-Ewing, Physical Review D **106**, 024014 (2022).
[24] M. Han and H. Liu, arXiv preprint arXiv:2212.04605 (2022).
[25] M. Han, C. Rovelli, and F. Soltani, Physical Review D **107**, 064011 (2023).
[26] T. Stachowiak and M. Szydłowski, Physics Letters B **646**, 209 (2007).
[27] A. Ashtekar and M. Bojowald, Classical and Quantum Gravity **23**, 391 (2005).
[28] L. Modesto, Classical and Quantum Gravity **23**, 5587 (2006).
[29] M. Bojowald and S. Brahma, Physical Review D **98**, 026012 (2018).
[30] D.-W. Chiou, Physical Review D—Particles, Fields, Gravitation, and Cosmology **78**, 044019 (2008).
[31] C. Zhang, Y. Ma, and J. Yang, Physical Review D **108**, 104004 (2023).
[32] J. Yang, C. Zhang, and Y. Ma, The European Physical Journal C **83**, 619 (2023).
[33] C.-Y. Shao, C. Zhang, W. Zhang, and C.-G. Shao, Physical Review D **109**, 064012 (2024).
[34] R.-B. Wang, S.-J. Ma, L. You, Y.-C. Tang, Y.-H. Feng, X.-R. Hu, and J.-B. Deng, arXiv preprint arXiv:2405.08241 (2024).

- [35] Z. Shi, X. Zhang, and Y. Ma, arXiv preprint arXiv:2408.15821 (2024).
- [36] M. A. Abramowicz and P. C. Fragile, *Living Reviews in Relativity* **16**, 1 (2013).
- [37] K. Giesel, B.-F. Li, and P. Singh, *Physical Review D* **104**, 106017 (2021).
- [38] V. Husain, J. G. Kelly, R. Santacruz, and E. Wilson-Ewing, *Physical Review Letters* **128**, 121301 (2022).
- [39] K. A. Meissner, *Classical and Quantum Gravity* **21**, 5245 (2004).
- [40] M. Domagala and J. Lewandowski, *Classical and Quantum Gravity* **21**, 5233 (2004).
- [41] D. Shukla, K. Pathak, *et al.*, arXiv preprint arXiv:2211.02008 (2022).
- [42] S. Hussain and M. Jamil, *Physical Review D* **92**, 043008 (2015).
- [43] R. ZNAJEK, *Nature* **262**, 270 (1976).
- [44] R. D. Blandford and R. L. Znajek, *Monthly Notices of the Royal Astronomical Society* **179**, 433 (1977).
- [45] D. Wang, K. Xiao, and W. Lei, *Monthly Notices of the Royal Astronomical Society* **335**, 655 (2002).
- [46] D.-X. Wang, R.-Y. Ma, W.-H. Lei, and G.-Z. Yao, *The Astrophysical Journal* **595**, 109 (2003).
- [47] A. Al Zahrani, V. P. Frolov, and A. A. Shoom, *Physical Review D—Particles, Fields, Gravitation, and Cosmology* **87**, 084043 (2013).
- [48] S. Koide, *Physical Review D* **67**, 104010 (2003).
- [49] S. Hussain, I. Hussain, and M. Jamil, *The European Physical Journal C* **74**, 1 (2014).
- [50] M. Jamil, S. Hussain, and B. Majeed, *The European Physical Journal C* **75**, 1 (2015).
- [51] B. Majeed, R. Rahim, and J. Rayimbaev, *Classical and Quantum Gravity* **40**, 115003 (2023).
- [52] V. P. Frolov, *Physical Review D—Particles, Fields, Gravitation, and Cosmology* **85**, 024020 (2012).
- [53] Q.-H. Huang, J.-H. Chen, and Y.-J. Wang, *Chinese Physics Letters* **31**, 060402 (2014).
- [54] I. D. Novikov and K. S. Thorne, *Black holes (Les astres occlus)* **1**, 343 (1973).
- [55] N. I. Shakura and R. A. Sunyaev, *Astronomy and Astrophysics*, Vol. 24, p. 337-355 **24**, 337 (1973).
- [56] A. H. Bokhari, J. Rayimbaev, and B. Ahmedov, *Physical Review D* **102**, 124078 (2020).
- [57] J. Rayimbaev, S. Shaymatov, and M. Jamil, *The European Physical Journal C* **81**, 1 (2021).
- [58] D. N. Page and K. S. Thorne, *Astrophysical Journal*, Vol. 191, pp. 499-506 (1974) **191**, 499 (1974).
- [59] B. Narzilloev and B. Ahmedov, *Symmetry* **14**, 1765 (2022).
- [60] J. M. Bardeen *et al.*, *Black holes* **215** (1973).
- [61] E. Kurmanov, K. Boshkayev, R. Giambò, T. Konysbayev, O. Luongo, D. Malafarina, and H. Quevedo, *The Astrophysical Journal* **925**, 210 (2022).
- [62] K. S. Thorne, *Astrophysical Journal*, Vol. 191, pp. 507-520 (1974) **191**, 507 (1974).
- [63] C. Bambi, *Black holes: a laboratory for testing strong gravity*, Vol. 10 (Springer, 2017).
- [64] J. E. McClintock, R. Shafee, R. Narayan, R. A. Remillard, S. W. Davis, and L.-X. Li, *The Astrophysical Journal* **652**, 518 (2006).
- [65] R. F. Penna, J. C. McKinney, R. Narayan, A. Tchekhovskoy, R. Shafee, and J. E. McClintock, *Monthly Notices of the Royal Astronomical Society* **408**, 752 (2010).
- [66] M. Heydari-Fard, M. Heydari-Fard, and H. R. Sepangi, *The European Physical Journal C* **81**, 473 (2021).
- [67] A. K. Kulkarni, R. F. Penna, R. V. Shcherbakov, J. F. Steiner, R. Narayan, A. Sądowski, Y. Zhu, J. E. McClintock, S. W. Davis, and J. C. McKinney, *Monthly Notices of the Royal Astronomical Society* **414**, 1183 (2011).
- [68] Q. Wang, M. Nowak, S. Markoff, F. Baganoff, S. Nayakshin, F. Yuan, J. Cuadra, J. Davis, J. Dexter, A. Fabian, *et al.*, *Science* **341**, 981 (2013).
- [69] S. Bhattacharyya, R. Misra, and A. V. Thampan, *The Astrophysical Journal* **550**, 841 (2001).
- [70] D. F. Torres, *Nuclear Physics B* **626**, 377 (2002).
- [71] I. Banerjee, B. Mandal, and S. SenGupta, *Monthly Notices of the Royal Astronomical Society* **500**, 481 (2021).
- [72] R. K. Karimov, R. Izmailov, A. Bhattacharya, and K. Nandi, *The European Physical Journal C* **78**, 1 (2018).
- [73] C. Liu, T. Zhu, Q. Wu, K. Jusufi, M. Jamil, M. Azreg-Ainou, and A. Wang, *Phys. Rev. D* **101**, 084001 (2020).
- [74] S. Brahma, C.-Y. Chen, and D.-h. Yeom, *Physical Review Letters* **126**, 181301 (2021).
- [75] M. Afrin, S. Vagnozzi, and S. G. Ghosh, *The Astrophysical Journal* **944**, 149 (2023).
- [76] S. Vagnozzi, R. Roy, Y.-D. Tsai, L. Visinelli, M. Afrin, A. Allahyari, P. Bambhaniya, D. Dey, S. G. Ghosh, P. S. Joshi, *et al.*, *Classical and Quantum Gravity* **40**, 165007 (2023).
- [77] S. Sahu, K. Lochan, and D. Narasimha, *Physical Review D* **91**, 063001 (2015).
- [78] J.-H. Chen and Y.-J. Wang, *Chinese Physics B* **20**, 030401 (2011).
- [79] M. Cruz, C. Silva, and F. Brito, *The European Physical Journal C* **79**, 1 (2019).
- [80] T. Zhu and A. Wang, *Physical Review D* **102**, 124042 (2020).

- [81] K. Jusufi and D. Stojkovic, *Universe* **8**, 194 (2022).
- [82] R. M. Wald, *General relativity* (University of Chicago press, 2010).

